Supporting Information for:

Developing Functionalized Fe_3O_4-Au Nanoparticles for Biomedical Application: a Physico-chemical Insight

Alessandra Luchini [(a,b)], Giuseppe Vitiello[(b,c)], Francesca Rossi[(d)], Odda Ruiz De Ballesteros[(a)], Aurel Radulescu[(e)], Gerardino D'Errico[(a,b)], Daniela Montesarchio[(a)], César de Julián Fernández [(d)], Luigi Paduano[(a,b)].*

[a] Dipartimento di Scienze Chimiche, Università degli Studi di Napoli "Federico II", Complesso Universitario di Monte S. Angelo, via Cintia, 80126 Naples, Italy.

[b] CSGI – Consorzio interuniversitario per lo sviluppo dei Sistemi a Grande Interfase, Italy.

[c] Dipartimento di Ingegneria Chimica, dei Materiali, e della Produzione Industriale, Università degli Studi di Napoli, "Federico II", Piazzale Tecchio 80, 80125 Naples, Italy.

[d] Institute of Materials for Electronics and Magnetism – Italian National Research Council
Parco Area delle Scienze 37/A - 43124 Parma, Italy.

[e] Jülich Centre for Neutron Science, Garching Forschungszentrum, Lichtenbergstrasse 1, D-85747 Garching bei München, Germany.

16LPC Functionalized NPs. Aiming to introduce biocompatible nanoparticles, the presented functionalization strategy was exploited to bind phospholipid molecules on nanoparticle surface. Two different phospholipids have purchased from Avanti Polar Lipids, 1-palmitoyl-2-hydroxy-*sn*-glycero-3-phosphocholine (16LPC 99%), or 1-octadecyl-2-hydroxy-*sn*-glycero-3-phosphocholine (18LPC 99%) at $4 \cdot 10^{-3}$ molal concentration were tested. The chosen phospholipids differ for their hydrocarbon chain length, which causes different aggregation tendency as indicated by their Critical Micelle Concentration (CMC) values of 4 to $8 \cdot 10^{-6}$ M for 16LPC and of $0.4 \cdot 10^{-6}$ M for 18LPC.[23 24] As reported in Figure SI1 (panel a) and in Table T1, two population distributions having mean hydrodynamic radius of about 10 and 60 nm are present in the 16LPC/NPs system. Dimensional considerations on the 16LPC coated nanoparticle suggests that the smallest distribution can be associated to the single functionalized nanoparticles, while the largest one is reasonably due to clusters formation.

The neutron scattering intensity profiles (Figure S2, panel b) were treated combining two different form factors in order to take into account the contribution arising from the nanoparticle clusters as

well as the single functionalized nanoparticles. In particular the experimental SANS data were fitted according to the following equations:

$$I(q) = \varphi_{core-shell} P_{core-shell}(q) + \varphi_{power-law} I_{power-law}(q) + \text{bkg} \quad (5)$$

Where:

$$P_{core-shell}(q) = \frac{scale}{V_{sphere}} \left[3V_c(\rho_c - \rho_s) \frac{\sin(qr_c) - qr_c \cos(qr_c)}{qr_c} + 3V_s(\rho_s - \rho_{solv}) \frac{\sin(qr_s) - qr_s \cos(qr_s)}{qr_s} \right] \quad (6)$$

being V_s= *shell volume,* V_c=*core volume,* r_s=*shell radius,* r_c= *core radius;*
and the power low*:*

$$I_{power-law}(q) = Aq^{-m} \quad (7)$$

and being φ the weight of the two contributions.

In particular in the case of the core-shell form factor, the core was considered as represented by both iron oxide and gold, while the organic layers, which are present on nanoparticle surface, represented the shell. Indeed, the scattering length density of gold and Fe_3O_4 iron oxide was calculated to be respectively $4.5 \cdot 10^{-6}$ Å^{-2} and $6.9 \cdot 10^{-6}$ Å^{-2}.Thus, the contrast between these two components was not sufficient to distinguish them using neutron scattering.

As summarized in Table T1, the parameters optimized by the fitting of the experimental curve confirmed the mass fractal structure of the nanoparticle cluster, since the power law exponential corresponded to -3. Furthermore, in the case of the single functionalized nanoparticles, the inorganic core (Fe_3O_4-Au) radius together with the organic shell thickness resulted in good agreement with the DLS results.

The major result of the DLS and SANS analysis is that the cluster formation process is affected by the aggregation of the amphiphilic molecule used for nanoparticle functionalization, and is related to their CMC, as reported above. In fact, the more hydrophobic 18LPC produces a more efficient and dense layer on the nanoparticle surface with respect to 16LPC, thus reducing the clustering propensity of 18LPC/NPS with respect to 16LPC/NPS. This effect could represent an appropriate tool to tailor functionalized nanoparticle system toward a specific size distribution.

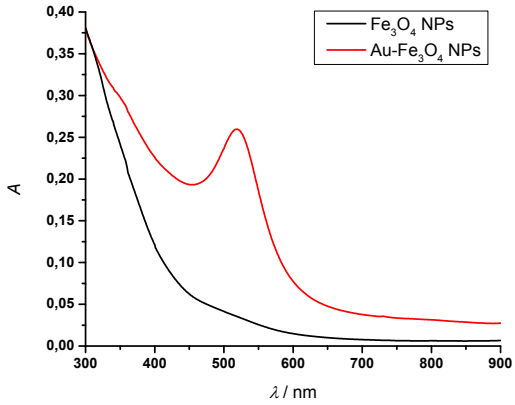

Figure SI1: *Comparison between UV-visible absorption spectra of Fe_3O_4 nanoparticle and Au-Fe_3O_4 nanoparticle suspensions.*

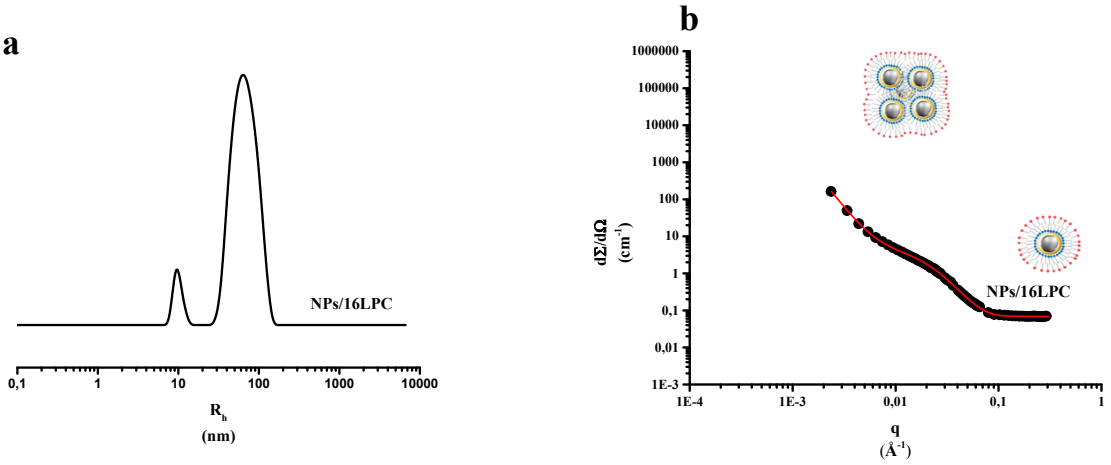

Figure SI2: *Hydrodynamic radius distributions 16LPC functionalized nanoparticle water suspensions (panel a). Neutron scattered intensity profiles obtained for 16LPC functionalized nanoparticles(panel b); the region where clusters and single functionalized contributions are prevalent is indicated.*

	$R_{h,NPs}$ (nm)	$R_{h,cluster}$ (nm)	R_{core} (nm)	d (nm)	$R_{cluster}$ (nm)
16/LPC	(9 ± 1)	(55 ± 2)	(4.0 ± 0.5)	(4.5 ± 0.5)	---

Table T1: *Hydrodynamic radius values obtained from Dynamic Light Scattering analysis and core radius and organic shell thickness obtained from Small Angle Neutron Scattering experiments. $R_{h,NPs}$ indicates the hydrodynamic radius of the single functionalized nanoparticle and $R_{h,cluster}$ is the hydrodynamic radius of the cluster. Furtherome, R_{core} is the inorganic nanoparticle radius, d is the thickness of the organic coating and $R_{cluster}$ is the radius of the cluster.*